Proceedings of the 11th ICPMG 2026
11th International Conference on Physical Modelling in Geotechnics
8-12 June 2026, Zurich, Switzerland

Development of a Numerical Analysis Model and Seismic Fragility Assessment for Railway Embankments

H.Song, M.Yoo, H.Kim
Gachon University, Seongnam, Republic of Korea, thdgusals12@gachon.ac.kr, mintaekyoo@gachon.ac.kr, khsss1026@gachon.ac.kr
J.Kim
Korea Railroad Research Institute (KRRI), Uiwang, Republic of Korea, jhkim06@krri.re.kr
W.Song
Urban Life Network, Daejeon, Republic of Korea, songws@urbanlife.or.kr
S.Haam
University of Seoul, Seoul, Republic of Korea, dandyhaam@uos.ac.kr

ABSTRACT: In this study, the dynamic behavior of railway embankments was analyzed using OpenSees, and seismic fragility functions were developed based on the results. For this purpose, a finite element–based numerical model was constructed by incorporating the Korean ground classification conditions. Since bedrock in most Korean sites is located within 30 m of the ground surface, the direct application of globally adopted site classification criteria may not accurately reflect local soil characteristics. Therefore, embankment height, bedrock depth, and shear wave velocity were selected as key parameters to represent Korean site conditions, and dynamic analyses were performed for a total of seven cases using recorded time-history ground motions. Based on the analysis results, seismic fragility functions were developed by defining the damage index in terms of the permanent vertical displacement of the embankment. Finally, the developed fragility functions were compared to evaluate the influence of each parameter on the seismic fragility of railway embankments.

1 INTRODUCTION

In recent years, high-magnitude earthquakes have occurred consecutively around the world. In Korea as well, the 2016 Gyeongju (Mw 5.8) and 2017 Pohang (Mw 5.4) earthquakes have raised public awareness of the need for earthquake preparedness. In particular, if seismic damage occurs to railway infrastructure facilities that are used daily by a large number of people, intercity transport and logistics networks could be paralyzed, potentially resulting in human casualties. Accordingly, seismic design and performance evaluation are essential to minimize earthquake damage to railway infrastructure facilities.

Among railway infrastructure facilities, an embankment is a structure constructed by compacting soil to maintain a consistent track elevation and to raise the railway line to the planned height in low-lying areas. Although it serves to ensure the stability of train operations, it is primarily composed of soil, making it highly susceptible to dynamic loads such as earthquakes. Therefore, the development of seismic fragility functions based on dynamic analyses is essential for the seismic design and performance evaluation of railway embankments.

Worldwide, dynamic numerical analyses of embankment behavior and the development of seismic fragility functions are being conducted. Mohammadi et al. (2023) conducted dynamic numerical analyses using the PLAXIS software to investigate the effects of soil material properties, embankment geometry, and both near-field and far-field ground motions. Seismic fragility functions were developed based on the derived permanent vertical displacement. Through this analysis, it was confirmed that seismic fragility increases as the internal friction angle and cohesion of the soil decrease, and that embankments with a greater height-to-width ratio exhibit higher fragility. In addition, it was shown that applying near-field ground motions results in a higher probability of embankment failure compared with far-field ground motions. Hubner and Mahler (2020) developed three embankment models with different heights and performed dynamic analyses using six recorded earthquake motions. Displacements were measured and used to develop seismic fragility functions, and it was confirmed that seismic fragility increases as the embankment height increases. Argyroudis and Kaynia (2015) conducted dynamic numerical analyses using five earthquake ground motions for embankments with varying heights on ground types classified as C and D, and developed seismic fragility functions based on the derived permanent vertical displacement. It was confirmed that seismic fragility increases with embankment height, and that embankments founded on ground type D exhibited higher fragility than those on ground type C. Oblak et al. (2020) analyzed the influence of various parameters on the response of embankments constructed on liquefiable soils and developed seismic fragility functions for each parameter. It was confirmed that seismic fragility increases with greater embankment height and width, and also increases as the thickness of the liquefiable layer increases or its density decreases. Zhou et al. (2022) developed seismic fragility functions for embankment structures considering different embankment heights and the application of liquefaction mitigation measures. The fragility functions were developed based on the permanent vertical displacement of the embankment, and it was observed that the probability of damage in all damage states increases with increasing embankment height. In addition, among the liquefaction mitigation measures, the installation of sheet piles was found to be the most effective in reducing the probability of damage.

Although numerous studies worldwide have been conducted on dynamic numerical analyses and the development of seismic fragility functions for embankment structures, research reflecting the ground classification conditions of Korea has been limited. Considering that bedrock depth at most Korean sites is within 30 m, applying globally adopted ground classification criteria could distort seismic fragility assessments for Korean ground conditions. Accordingly, in this study, seven analysis cases were established by setting bedrock depth, soil shear wave velocity, and embankment height as variables considering Korea's ground classification conditions, and dynamic analyses were conducted using OpenSees. For each case, the permanent vertical displacement of the embankment was measured, and seismic fragility functions were developed by defining damage index and threshold values based on Korean standards. The effects of each variable were then comparatively analyzed.

2 DYNAMIC NUMERICAL ANALYSIS OF RAILWAY EMBANKMENTS

2.1 Numerical modeling of railway embankments

In this study, a two-dimensional finite element model under plane strain conditions was developed using OpenSees to derive seismic fragility functions for railway embankments. The analysis cases were constructed based on the five ground types (S1–S5) specified in the Korean seismic design standard, General Seismic Design (KDS 17 10 00). The shear wave velocities of the soil layers were determined using the average values obtained from the embankment sections of the Honam High-Speed Railway, in accordance with the bedrock depth conditions defined for each ground type in KDS 17 10 00. The ground classification conditions in Korea are summarized in Table 1 and the analysis cases constructed in this study are presented in Table 2.

The height of the embankment was set to 8 m for Cases 1 through 5, while Cases 6 and 7 were configured with heights of 3 m and 6 m, respectively, to compare the fragility according to embankment height. In this context, the analysis conditions for Cases 6 and 7 were identical to those of Case 5, except for the embankment height. In addition, the crest length was set to 16 m for all analysis cases, and the shear wave velocity of the embankment was assigned as 290 m/s. The embankment slope was set to 1:1.8, which is the standard slope for railway embankments specified in the Korean Geotechnical Design Standard for Embankment and Cut (KDS 11 70 05) based on the high-speed railway design criteria.

Table 1. Ground classification Criteria (KDS 17 10 00)

Soil Type	Description of soil	Classification Criteria	
		Bedrock Depth, H (m)	Shear Wave Velocity (m/s)
S_1	Rock	H <1	-
S_2	Shallow, stiff soil	1≤ H ≤20	≥260
S_3	Shallow, soft soil		≤260
S_4	Deep, stiff soil	H >20	≥180
S_5	Deep, soft soil		≤180

Table 2. Analysis Case

Case No.	Embankment height (m)	Bedrock Depth (m)	Shear Wave Velocity (m/s)	Soil Type
1	8	1	330	S_1
2	8	13	330	S_2
3	8	13	200	S_3
4	8	28	280	S_4
5	8	28	160	S_5
6	3	28	160	S_5
7	6	28	160	S_5

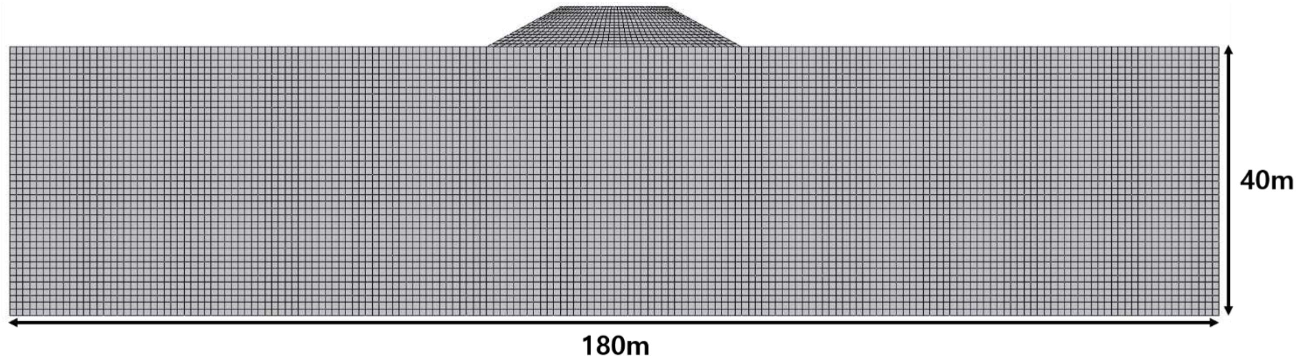

Figure 1.model cross-section of embankment structure

The modeled analysis cross-section is shown in Figure 1. To determine an appropriate model width that minimizes boundary effects on the crest response, a sensitivity analysis was conducted by increasing the model width to 140 m, 180 m, and 220 m. For this comparison, the Kobe ground motion scaled to a peak ground acceleration (PGA) of 0.30 g was applied. The resulting permanent vertical displacements at the central crest were 0.175 m, 0.180 m, and 0.181 m, respectively. Based on these results, the crest response was judged to be converged from a model width of 180 m. Therefore, a model width of 180 m was adopted. The total model height was set to 40 m. Depending on the bedrock depth of each analysis case, the upper layer was modeled as soil and the lower layer as rock.

The model was composed of four-node quadrilateral elements under two-dimensional plane strain conditions, with two degrees of freedom assigned to each node. The element size (h) was determined based on the shear wave velocity (V_s) and the target maximum frequency (f_{max}) by calculating the wavelength as expressed in Equation (1). Following the recommendation of Kuhlemeyer and Lysmer (1973), the element size was set to satisfy the condition given in Equation (2). For a conservative design, the element size was evaluated based on Case 5, which had the lowest shear wave velocity, and accordingly, the element size was set to 1 × 1 m for all analysis cases. At the soil–rock interface, the same element size of 1 m was maintained to avoid numerical instability associated with mesh size discontinuity. Under this mesh configuration, the key responses at the central crest of the embankment, including acceleration and permanent vertical displacement, exhibited numerically stable behavior during the analyses.

$$\lambda = V_s/f_{max} \quad (1)$$

$$h \leq \lambda/10 \quad (2)$$

The boundary conditions of the model were also set identically for all analysis cases. For the bottom boundary nodes where the seismic waves were applied, the horizontal degree of freedom was left free to input horizontal ground motion, while the vertical degree of freedom was fixed. The left and right boundaries were connected by applying the equalDOF (equal degrees of freedom) condition between nodes at the same elevation to simulate an infinite ground domain. All other nodes were assigned free boundary conditions in both the horizontal and vertical degrees of freedom, allowing dynamic responses to occur.

Prior to the fragility analysis, a preliminary check was conducted to confirm the physical plausibility of the numerical model. For this purpose, Cases 4 and 5, which have identical embankment height and bedrock depth but different shear wave velocities, were subjected to the Kobe earthquake record scaled to a PGA of 0.30 g, and the responses at the central crest of the embankment were compared. The results showed that the softer case (Case 5) exhibited a larger peak acceleration at the central crest of 0.464 g and a greater permanent vertical displacement of 0.180 m, whereas Case 4 showed a peak acceleration of 0.408 g and a permanent vertical displacement of 0.045 m, which is consistent with the generally observed trend of increased dynamic amplification and deformation under relatively softer ground conditions.

2.2 Input parameters of soil and rock layers

In this study, both the embankment and the underlying soil layer were modeled as single-layer sandy soils, and the PressureDependMultiYield (PDMY) model (Yang et al., 2003) was employed to simulate the nonlinear behavior of sand. The main input parameters included density, shear modulus, and bulk modulus, which were calculated based on the shear wave velocity and Poisson's ratio of the soil layer for each analysis case. The representative input parameters corresponding to each shear wave velocity are summarized in Table 3.

Table 3. PDMY parameters

Parameters	Vs= 160m/s	Vs= 200m/s	Vs= 280m/s
Density (ton/m^3)	1.7	1.75	1.9
Poisson's ratio	0.38	0.35	0.3
Shear Modulus (kPa)	43,520	70,000	148,960
Bulk Modulus (kPa)	166,826.7	210,000	322,746.7

Parameters	Vs= 290m/s	Vs= 330m/s
Density (ton/m^3)	1.91	1.95
Poisson's ratio	0.29	0.27
Shear Modulus (kPa)	160,631	212,355
Bulk Modulus (kPa)	328,911.1	390,856.3

Table 4. Rock parameters

Parameters	Value
Elastic modulus (kPa)	3,600,000
Poisson's ratio	0.2
Density (ton/m^3)	2.34

The underlying rock layer was modeled using the ElasticIsotropic model (Mazzoni et al., 2007). The input parameters included the elastic modulus, Poisson's ratio, and density, which were calculated and applied based on a shear wave velocity of 800 m/s. The material properties of the rock used in the analysis are presented in Table 4.

2.3 Input ground motion

A total of five recorded time-history ground motions were selected for the dynamic analysis to represent a range of frequency characteristics. The selected ground motions were the 1968 Hachinohe earthquake, the 1994 Northridge earthquake, the 1995 Kobe earthquake, the 1999 Kocaeli earthquake, and the 2017 Pohang earthquake. In particular, considering that the analyses were conducted based on the Korean ground classification criteria, the recorded ground motion from the 2017 Pohang earthquake, which occurred in Korea, was included.

Each ground motion was scaled based on the PGA from 0.05 g to 0.5 g in increments of 0.05 g, resulting in 50 nonlinear dynamic time-history analyses for each analysis case.

2.4 Dynamic analysis

Dynamic analyses were performed to evaluate the permanent vertical displacement at the central crest of the embankment for developing seismic fragility functions for railway embankments. To establish the initial stress distribution, an elastic gravity analysis was first conducted by applying the unit weight vertically to each element. Subsequently, a plastic gravity analysis was performed to transfer the initial stress state obtained from the elastic analysis to the nonlinear material behavior. In the dynamic analyses, Rayleigh damping was adopted, with target damping ratios assigned separately to each material domain. A damping ratio of 5% was applied to the embankment and underlying soil layers, while a damping ratio of 0.5% was assigned to the bedrock.

Afterward, the recorded time-history ground motions were applied to the model, and dynamic analyses were performed to obtain the permanent vertical displacement. In this step, the permanent vertical displacement induced by dynamic loading was calculated as the difference between the displacement immediately after the gravity analysis and that at the end of the dynamic analysis.

3 DEVELOPMENT OF SEISMIC FRAGILITY FUNCTIONS

3.1 Methodology for the development of seismic fragility functions

For all analysis cases, dynamic analyses were performed using a total of 50 recorded time-history ground motions to develop seismic fragility functions. Based on the permanent vertical displacement results at the central crest point of the embankment obtained from each analysis, the probability of exceeding each damage state was calculated with respect to the PGA. The PGA was determined from the acceleration time histories at the free-field ground surface, using the maximum absolute value of the acceleration.

The damage index and threshold values for calculating the exceedance probability of damage were defined based on the permanent vertical displacement at the central crest point of the embankment, with reference to the high-speed railway track irregularity management criteria specified in the Guidelines for Railway Track Maintenance (Ministry of Land, Infrastructure and Transport, 2019). The damage index (DI) was calculated using the permanent vertical displacement at the central crest point of the embankment (D) and the minimum threshold of 0.01 m specified in the track settlement warning criteria, as expressed in Equation (3). The damage indices corresponding to each damage state are presented in Table 5.

$$\mathrm{DI} = \mathrm{D}/0.01 \quad (3)$$

Table 5. Definition of Damage States and Damage Indices

Damage state	Management Levels of Vertical Track Irregularity	Damage Index
Minor	Warning level	1≤ DI <1.8
Moderate	Maintenance level	1.8≤ DI <3
Extensive	Speed Restriction Level	3≤ DI <30

Using the damage index and damage thresholds, the seismic fragility functions were formulated by the lognormal cumulative distribution function, as expressed in Equation (4).

$$\mathrm{P}_f(ds \geq ds_i|S) = \Phi(\frac{\ln (IM/IM_{mi})}{\beta_{tot}}) \quad (4)$$

P_f represents the probability of exceeding a specific damage state with respect to the ground motion intensity, which was calculated in this study using the PGA. Φ denotes the standard normal cumulative distribution function, Im_{mi} is the median intensity measure causing the *i*-th damage state, and β_{tot} represents the lognormal standard deviation.

For each damage state, Im_{mi} was derived through a linear regression analysis of the relationship between the PGA and the damage index, based on the results of the 50 recorded time-history ground motions analyses conducted in this study. In cases where the analysis results did not reach the threshold for extensive damage, the corresponding values were estimated by extrapolation based on the regression equation. The total variability, β_{tot}, was calculated as shown in Equation (5), considering the uncertainty due to response variability from ground motion (β_D), the uncertainty in the definition of damage states (β_{ds}), and the uncertainty associated with the structural capacity (β_c). β_{ds} was set to 0.4, as defined for buildings in FEMA (2004), and β_c was set to 0.3 according to Argyroudis and Kaynia (2015).

$$\beta_{tot} = \sqrt{\beta_D^2 + \beta_{ds}^2 + \beta_c^2} \quad (5)$$

3.2 Suggested seismic fragility functions

The median and standard deviation of the lognormal cumulative distribution parameters for each damage state, derived from the analysed cases, are presented in Table 6. Among all analysis cases, the seismic fragility function for Case 5 is presented in Figure 2 as a representative example.

Table 6. Parameters of the Seismic Fragility Functions

Case No.	Median		
	Minor	Moderate	Extensive
1	0.621	0.833	2.384
2	0.382	0.529	1.694
3	0.286	0.363	0.854
4	0.256	0.348	1.035
5	0.224	0.281	0.638
6	0.247	0.309	0.692
7	0.235	0.294	0.658

Case No.	Standard deviation		
	Minor	Moderate	Extensive
1	0.594	0.594	0.594
2	0.626	0.626	0.626
3	0.543	0.543	0.543
4	0.561	0.561	0.561
5	0.549	0.549	0.549
6	0.535	0.535	0.535
7	0.545	0.545	0.545

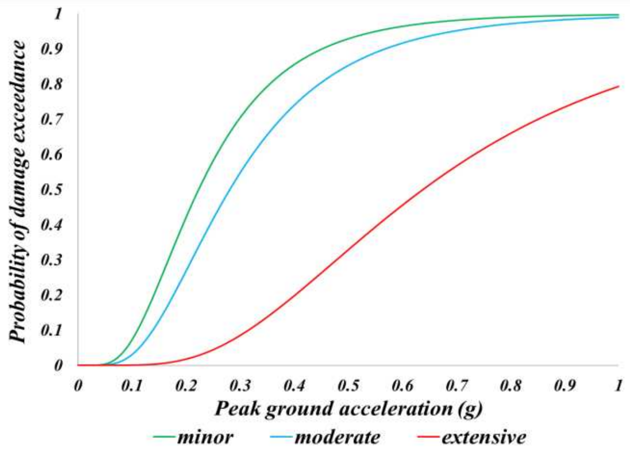

Table 6. Seismic fragility function of Case 5 (Representative Case)

Comparison of Cases 1 through 5 indicates that seismic fragility was highest for Case 5 (ground type S_5), followed in descending order by Case 4 (S_4), Case 3 (S_3), Case 2 (S_2), and Case 1 (S_1). A comparison between Case 1 and Case 2, which have identical shear wave velocities in the underlying soil layer, shows that Case 1 exceeds a 50% probability of moderate damage at PGA levels above 0.833 g, while Case 2 does so at levels above 0.529 g. This indicates that even with identical shear wave velocities in the underlying soil layer, the thickness of the soil layer influences the seismic fragility, with greater thickness leading to higher fragility. Similarly, a comparison between Case 4 and Case 5, which have the same soil thickness, shows that Case 4 exceeds a 50% probability of moderate damage at PGA levels above 0.348 g, while Case 5 does so at levels above 0.281 g. This result indicates that lower shear wave velocity in the underlying soil layer leads to higher seismic fragility. These results indicate that an increase in the thickness of the underlying soil layer or a decrease in its shear wave velocity reduces the fundamental frequency of the ground, thereby increasing the likelihood of resonance with the low-frequency components of the input ground motion and consequently amplifying the seismic fragility of the railway embankment.

Furthermore, to analyze the effect of embankment height, Cases 6, 7 and 5 corresponding to embankment heights of 3 m, 6 m, and 8 m, respectively, were compared. The PGA values at which the probability of moderate damage exceeded 50% were 0.309 g for Case 6, 0.294 g for Case 7, and 0.281 g for Case 5, indicating that the seismic fragility of the railway embankment increases progressively with embankment height.

The results of the seismic fragility functions indicate that, among the underlying soil conditions, soil thickness and shear wave velocity had the greatest influence on seismic fragility, while the embankment height also affected it. Therefore, in the seismic design and performance evaluation of railway embankments, not only the thickness and shear wave velocity of the underlying soil but also the effect of embankment height should be comprehensively considered.

4 CONCLUSIONS

In this study, a two-dimensional finite element model of a railway embankment was developed considering the ground classification conditions in Korea, and seismic fragility functions were derived for a total of seven analysis cases. For the underlying ground, the bedrock depth and shear wave velocity of the soil layer were varied to reflect the conditions of the Honam High-Speed Railway embankment section in Korea. For the embankment, different heights were applied, and the standard slope for high-speed railway embankments specified in the Korean design standards was reflected. Based on the developed model, dynamic analyses were performed using 50 recorded ground motions to evaluate the permanent vertical displacement. With reference to the Korean Track Maintenance Guidelines, the damage index and damage thresholds were defined from the permanent vertical displacement, and seismic fragility functions were derived by linear regression analysis.

The analysis of the seismic fragility functions indicated that bedrock depth and shear wave velocity of the soil, which are key parameters in Korea's ground classification, were the dominant factors influencing the seismic fragility of the railway embankments. Under identical bedrock depth conditions, seismic fragility increased as the soil shear wave velocity decreased, while under identical shear wave velocity conditions, greater bedrock depth, corresponding to increased soil layer thickness, led to higher seismic fragility. This is attributed to the decrease in the fundamental frequency of the soil layer as its shear wave velocity decreases or its thickness increases, which increases the likelihood of resonance with the low-frequency components of the input ground motion, thereby amplifying the seismic fragility of the embankment structure. In addition, under identical underlying ground conditions, it was confirmed that seismic fragility increases with increasing embankment height.

These findings highlight the necessity of developing analysis models that reflect Korea's ground classification conditions for the seismic design and performance evaluation of railway embankments. Since the bedrock depth in most Korean ground conditions is within 30 m, applying foreign ground classification criteria may distort the seismic fragility assessment of actual Korean ground conditions. Therefore, this study is significant in that it developed seismic fragility functions for railway embankments based on Korea's ground classification conditions and actual design guidelines. However, future research will consider multilayered ground conditions to conduct more detailed dynamic analyses and develop refined seismic fragility functions, thereby providing fundamental data for seismic design and performance evaluation.

ACKNOWLEDGEMENTS

Funding: This research was supported by the Korea Agency for Infrastructure Technology Advancement (KAIA) grant funded by the Ministry of Land, Infrastructure and Transport (Grant No. RS-2023-00238458) and by the Korea Railroad Research Institute (KRRI) Basic Research Program (Development of Intelligent Information-Based Technologies for Complex Disaster Response to Extreme Climate Events, PK26414A0). The authors gratefully acknowledge this financial support.

REFERENCES

Mohammadi, M., Mosleh, A., Razzaghi, M. S., Alves Costa, P., and Calçada, R. (2023). Probabilistic seismic safety assessment of railway embankments. *Applied Sciences*, Vol. 13, No. 1, p. 598.

Hübner, B., and Mahler, A. (2020). Analysis of seismic fragility functions of highway embankments. *Periodica Polytechnica Civil Engineering*, Vol. 64, No. 4, pp. 1162–1169.

Argyroudis, S., and Kaynia, A. M. (2015). Analytical seismic fragility functions for highway and railway embankments and cuts. *Earthquake Engineering & Structural Dynamics*, Vol. 44, No. 11, pp. 1863–1879.

Oblak, A., Kosič, M., Viana Da Fonseca, A., and Logar, J. (2020). Fragility assessment of traffic embankments exposed to earthquake-induced liquefaction. *Applied Sciences*, Vol. 10, No. 19, p. 6832.

Zhou, H., Liu, X., Tan, J., Zhao, J., and Zheng, G. (2023). Seismic fragility evaluation of embankments on liquefiable soils and remedial countermeasures. *Soil Dynamics and Earthquake Engineering*, Vol. 164, p. 107631.

Ministry of Land, Infrastructure and Transport (MOLIT). (2018). *General seismic design (KDS 17 10 00)*. Ministry of Land, Infrastructure and Transport, Sejong, Korea (in Korean).

Ministry of Land, Infrastructure and Transport (MOLIT). (2016). *Embankment and cut (KDS 11 70 05)*. Ministry of Land, Infrastructure and Transport, Sejong, Korea (in Korean).

Kuhlemeyer, R. L., and Lysmer, J. (1973). Finite element method accuracy for wave propagation problems. *Journal of the Soil Mechanics and Foundations Division*, Vol. 99, No. 5, pp. 421–427.

Yang, Z., Elgamal, A., and Parra, E. (2003). A computational model for cyclic mobility and associated shear deformation. *Journal of Geotechnical and Geoenvironmental Engineering*, Vol. 129, No. 12, pp. 1119–1127.

Mazzoni, S., McKenna, F., Scott, M. H., and Fenves, G. L. (2007). *OpenSees Command Language Manual*. Pacific Earthquake Engineering Research (PEER) Center, University of California, Berkeley.

Ministry of Land, Infrastructure and Transport (MOLIT). (2019). *Guidelines for railway track maintenance*. Ministry of Land, Infrastructure and Transport, Sejong, Korea (in Korean).

FEMA (2004). HAZUS-MH: User’s Manual and Technical Manuals. National Institute of Building Sciences, prepared for the Federal Emergency Management Agency, Washington, D.C., USA.